JOURNAL OF Materials CHEMISTRY

Theoretical calculations on the structures, electronic and magnetic properties of binary 3d transition metal nitrides

Bernhard Eck,[a] Richard Dronskowski,*[a] Masao Takahashi[b] and Shinichi Kikkawa[b]

[a]*Institut für Anorganische Chemie, Rheinisch-Westfälische Technische Hochschule, Prof.-Pirlet-Str. 1, 52074 Aachen, Germany. E-mail: drons@HAL9000.ac.rwth-aachen.de*
[b]*The Institute of Scientific and Industrial Research, Osaka University, 8–1, Mihogaoka, Ibaraki, Osaka 567, Japan*

Received 21st December 1998, Accepted 12th April 1999

The electronic structures of a number of binary 3d transition metal and iron nitrides, some of which still need to be synthesized, have been investigated by means of spin-polarized first principles band structure calculations (TB-LMTO-ASA). The chemical bonding in all compounds has been clarified in detail through the analysis of total and local densities-of-states (DOS) and crystal orbital Hamilton populations (COHP). The binary transition metal nitride set includes ScN, TiN, VN, CrN, MnN, FeN, CoN and NiN, both in the sodium chloride as well as in the zinc blende structure type. Antibonding metal–metal interactions for higher electron counts are significantly weaker in the zinc blende type, thus favoring this structural alternative for the later transition metal nitrides.

For binary iron nitrides, the stoichiometric phases α''-$Fe_{16}N_2$, γ'-Fe_4N, ε-Fe_3N, ζ-Fe_2N as well as the recently synthesized (rf-sputtering) non-stoichiometric compounds γ''-$FeN_{0.91}$ and γ'''-$FeN_{0.5-0.7}$ have been investigated. There is experimental evidence that γ''-$FeN_{0.91}$ adopts the zinc blende structure type while γ'''-$FeN_{0.5-0.7}$ should crystallize in a defect sodium chloride type structure. For the stoichiometric phases, most numerical theoretical data are consistent with the measured ground state properties (lattice parameters and magnetic moments) whenever experimentally available. The general trends concerning iron–nitrogen and iron–iron bonding have been elucidated; the role of nitrogen vacancies were simulated by a number of model calculations. It appears that potentially antibonding interactions are the source of local structural distortions in all of these phases.

For γ''-$FeN_{0.91}$, theory supports the proposed metallic zinc blende structure with a theoretical lattice parameter of 421 pm for the exact 1 : 1 composition. With respect to γ'''-$FeN_{0.5-0.7}$ in the defect NaCl structure type, we arrive at theoretical lattice constants between 389 and 398 pm, somewhat depending upon the nitrogen content.

1 Introduction

The chemistry and physics of the iron and other transition metal nitrides are of fundamental importance for both basic research and technology, *i.e.* steel production and hardening. As early as 1951, for example, Jack delivered the first definite phase diagram for the iron nitrides.[1] He is also responsible for the first synthesis of these solid state materials. Since then additional efforts, aimed at further *understanding* of these compounds, have only been made within the last couple of years.

Indeed, the iron nitrides as well as other transition metal nitrides have found significant interest in solid state chemistry not too long ago. There are possible applications for transition metal nitrides as materials for magnetic storage devices, superconductors, or in the semiconductor industry, where the nitrides may replace the established oxides because of superior properties in some cases. Besides that, there is the promising class of silicon nitride based ceramics which is utilized by materials scientists in various engineering applications.

If compared with the extraordinarily large number of transition metal oxides, the relatively small number of the corresponding nitrides is puzzling. This can, however, be easily traced back to the much more challenging techniques required to prepare nitride phases. It is generally hoped that the search for new nitrides with superior properties (see above) may be supported by computational techniques. Inspired by this goal, we present a detailed study of the chemical bonding in iron and other transition metal nitrides, based upon *ab initio* band structure calculations.

2 Methods

Electronic structure calculations were performed using *ab initio* all-electron techniques with scalar-relativistic corrections. The specific method used was Linear Muffin-Tin Orbital (LMTO) theory[2–4] which is a fast linearized form of the KKR method.[5,6] It accounts for the potential from all the electrons and is applicable to materials composed of atoms from any part of the Periodic Table. The almost minimal, unfixed LMTO basis sets adjust dynamically to the respective potentials. While the wave functions of the valence electrons are expanded into Hankel envelope functions in the interstitial regions with flat potentials, numerical solutions of the radial Dirac equation are computed in the core-like regions.

The electronic energy was calculated *via* spin density-functional theory, replacing the many-particle problem by the self-consistent solution of the Kohn–Sham equations,[7,8] parameterized according to von Barth and Hedin.[9] Diagonalization and integration in reciprocal space was performed with the help of an improved tetrahedron method.[10] All calculations were checked for convergence of energies, orbital moments, integrated Crystal Orbital Hamilton Population (COHP) values, and, where appropriate, magnetic moments with respect to the number of k points. The energies were converged at least within 10^{-5} Ry, the magnetic moments at least within 0.04 μ_B. The basis set of short-ranged[11] atom-centered TB-LMTOs contained s–d valence functions for the transition metals and s–p for the nitrogen atoms. When necessary, 'empty spheres' (atomic wave functions without nuclei) were incorporated into the cell in order to increase variational freedom and improve packing. Starting from

atomic Hartree potentials, the structures were then iterated by use of the atomic-spheres approximation (ASA), employing muffin-tin spheres blown up to overlapping and volume filling spheres. Optimizations of the lattice constants were performed in the non-spin-polarized mode and further checked using spin polarization in some cases; they did not improve by more than 1–3 pm. Finally, spin-polarized calculations were carried out at the optimized lattice constants. To do so, a small perturbation was introduced into the two spin sublattices by manually changing their occupations. In the following, the electronic structure was then again iterated towards self-consistency, either converging to a non-magnetic (no unpaired electrons) or a magnetic (fractional occupations for the spin sublattices) ground state.

The above method is well established in solid state chemistry and physics; for ground state properties such as cohesive energies, lattice constants or magnetic moments it can be expected to yield satisfactory results that match accurate experimental data. The program used was TB-LMTO 4.7.[12]

The chemical bonding in all phases was investigated using Crystal Orbital Hamilton Population (COHP) analysis.[13] This technique provides information analogous to the familiar Crystal Orbital Overlap Population (COOP) analysis[14] used in extended Hückel calculations.[15] While COOP curves are energy resolved plots of the Mulliken overlap population between two atoms or orbitals, a COHP curve is an energy resolved plot of the contribution of a given bond to the bonding energy of the system. There is one very important difference between COHP and COOP curves: while COOPs are usually presented as an *average* of several bonds, COHPs typically include the *sum* of those bonds. While this does not affect the shape of COHP curves, it does change their size. All COHP curves are presented here in a format similar to COOP curves: positive values are bonding, and negative antibonding (*i.e.* we are plotting $-$COHP instead of COHP).

3 Results

3.1 Binary 1 : 1 transition metal nitrides

It was long believed that all of the simple 1 : 1 binary 3d transition metal nitrides should crystallize in the sodium chloride structure type, even though only the early transition metal nitrides (Sc to Cr) had been synthesized.[16–19] FeN and CoN have only recently been prepared,[20–22] and their structures were determined to be of the zinc blende type.

There have been calculations reported for this particular class of compounds, carried out with a combination of *ab initio* total-energy techniques (using the LMTO method) and thermodynamic data analysis.[23] It was found that MnN in the sodium chloride structure should have the smallest cohesive energy of all binary 3d transition metal nitrides. Unfortunately, these calculations were restricted to the sodium chloride structure type, and alternative structures were not examined. In the following, we will analyze both the sodium chloride and the zinc blende structure types.

ScN,[16] TiN,[17] VN,[18] and CrN[19] crystallize in the sodium chloride structure type; for numerical data, see Table 1. Here, the transition metals (as well as the nitrogens) experience six-fold coordination with metal–nitrogen distances of 220 pm (ScN), 212 pm (TiN), 205 pm (VN) and 207 pm (CrN). The twelve second-nearest neighbor distances are 311 pm (Sc–Sc), 300 pm (Ti–Ti), 290 (V–V) and 293 pm (Cr–Cr). FeN[21] and CoN[20] both adopt the zinc blende structure type and have essentially the same lattice constants. The metal and nitrogen atoms in these structures are tetrahedrally coordinated, with metal–nitrogen distances of 186 pm. The twelve second-nearest-neighbor contacts are 304 pm long. Both compounds are considered to be stoichiometric, with nitrogen contents of 49.5 and 50.2%, respectively. From a theoretical perspective, it is very interesting to ask what structures are expected for MnN and NiN, which have yet to be synthesized.

Since the DOS and COHP curves of MN (M = Sc–Ni) are quite similar to those of FeN, we may adopt a rigid band model. Thus, we show the DOS of FeN in the sodium chloride (Fig. 1) and zinc blende (Fig. 2) structures along with arrows indicating the position of the Fermi energy ε_F for the other isostructural compounds. The behavior of ε_F across the series is what we would expect: moving up through the bands as the atomic number (and thus the number of valence electrons) increases. Iron–nitrogen and iron–iron COHPs for FeN on both structure types are also shown in Fig. 1 and 2.

In both structures of FeN, there are two sets of peaks in the DOS. The first, centered at *ca.* -6 eV, is primarily composed of nitrogen 2p orbitals, with a bonding admixture of iron 3d. The iron–nitrogen antibonding peak in which ε_F is located is mostly iron 3d in character. The familiar three below two (t_{2g} below e_g) crystal field splitting pattern we would expect for octahedral iron in the sodium chloride structure is obscured by the large dispersion of the 3d peaks in the DOS. In the zinc blende structure, however, the 3d peaks are narrow enough for the e below t_2 crystal field splitting to be discerned. As we would expect, the iron–nitrogen π^* interactions in the e set (centered at *ca.* -2 eV) are considerably weaker than the σ^* interactions in the t states centered at *ca.* 2.5 eV.

The integrated iron–nitrogen COHPs in the sodium chloride (-3.50 eV bond^{-1}) and zinc blende (-4.04 eV bond^{-1}) structures are very nearly the same for FeN. To understand the difference in stability between these two structures, we need to consider the iron–iron interactions (Fig. 1 and 2). The iron–iron contacts in the sodium chloride structure (279 pm) are considerably shorter than those in the zinc blende structure (297 pm). This fact is reflected in the magnitude of the iron–iron COHP curves (-0.21 eV bond^{-1} for sodium chloride, -0.03 eV bond^{-1} for zinc blende). Note the relatively strong iron–iron antibonding interactions around ε_F in the sodium chloride structure.

Transformations to the zinc blende structure type considerably lessens the strength of those interactions. Their total amount, however, cannot be structurally decisive whereas iron–iron antibonding interactions at the Fermi level seem to be more critical: in the earlier members of the MN series, the Fermi level lies lower in the metal–metal COHP curve, not yet

Table 1 Crystallographic and theoretical data for ScN, TiN, VN, CrN, FeN and CoN

Compound	Structure type (space group)	Experimental		Theoretical	
		a/pm	μ_B	a/pm	μ_B
ScN	NaCl ($Fm\bar{3}m$)	444[16]		446	0
TiN	NaCl ($Fm\bar{3}m$)	423.9[17]		424	0
VN	NaCl ($Fm\bar{3}m$)	410[18]		410	0
CrN	NaCl ($Fm\bar{3}m$)	414.0[19]		402	1.4
FeN	ZnS ($F\bar{4}3m$)	430.7[21] (FeN) 433[22] (γ''-$FeN_{0.91}$)	AF or 0	420	0
CoN	ZnS ($F\bar{4}3m$)	429.7[20]	para	422	0

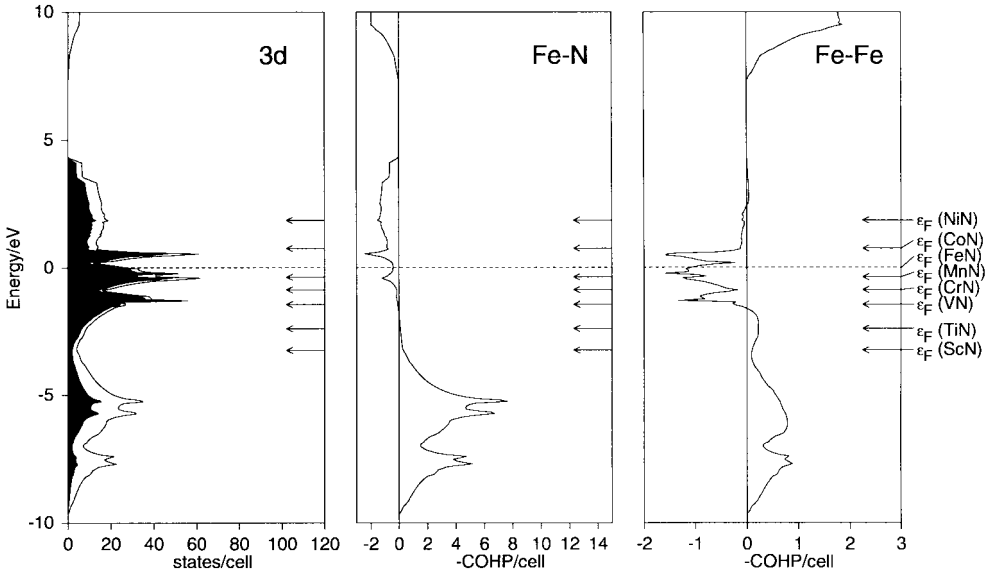

Fig. 1 Density-of-states (DOS) and local 3d projections (left), and the Crystal Orbital Hamilton Populations for the iron–nitrogen interactions (middle) and the iron–iron interaction (right) in FeN for the sodium chloride structure. The arrows denote the Fermi levels in the other isostructural compounds.

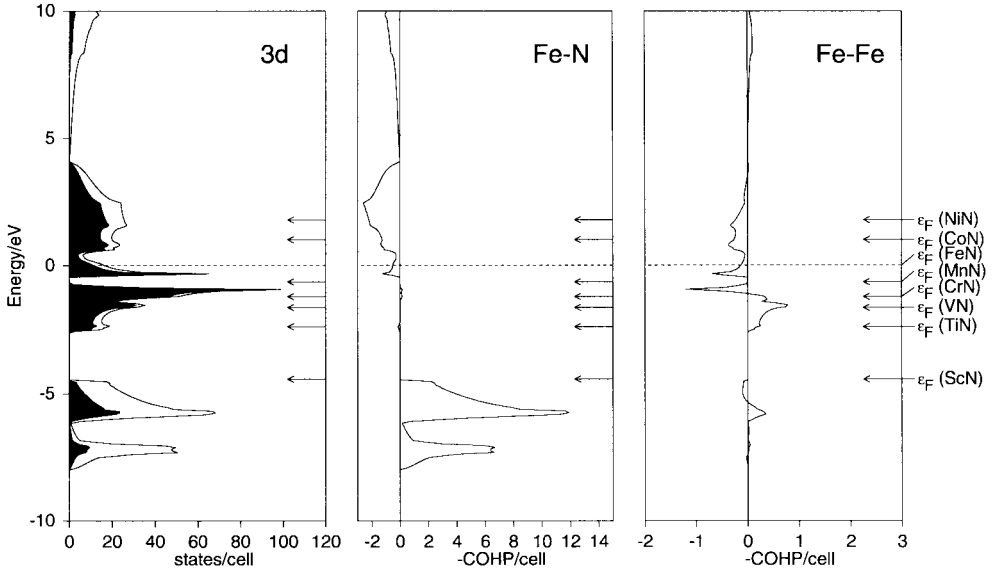

Fig. 2 Same as Fig. 1 but for the zinc blende structure.

sampling so many antibonding states. For these electron counts the sodium chloride structure, with much shorter metal–metal contacts, is favored. For higher electron counts, switching to the zinc blende structure type reduces these antibonding interactions by a significant amount.

Based upon this simple bonding analysis, we predict that MnN should appear in the zinc blende structure type. NiN is a little bit more problematic. Here ε_F is quite high in both the nickel–nitrogen and the nickel–nickel COHP curves. Many antibonding levels are populated in either structure type, leading us to doubt the stability of this compound, a conclusion in agreement with a thermodynamic analysis.[24]

Looking at the integrated COHP values for an iron–nitrogen octahedron, the values for the sodium chloride structure increase from ScN to FeN, and then decrease (Table 2). The values for the zinc blende structure show the same behavior but with smaller differences, leading to a nearly similar value for NiN. It is dangerous to overstress these qualitative arguments, however, a plot of the difference of the ICOHPs between the two structure types for a *single* metal–nitrogen bond (Fig. 3) is suggestive. The more positive this difference, the more stable is a *single* bond in the zinc blende structure compound. One can see that the difference is small (<0.26 eV) for ScN–CrN, while for MnN–NiN the difference is >0.45 eV. The large energy difference for MnN (close to the FeN value) also supports our prediction of the zinc blende structure for MnN. If NiN is indeed stable enough to be synthesized (see above), it will be found in the zinc blende and not in the sodium chloride structure, unless a completely different structure type, unknown to us, would be favored.

Concerning the calculated magnetic moments, we found zero unpaired electrons for ScN, TiN and VN, 1.4 for CrN, 2.2 for MnN, 1.3 for FeN, and again zero for CoN and NiN, assuming a sodium chloride structure. For the zinc blende structure, the calculated values are zero for ScN and TiN, 0.1 for VN, 1.0 for CrN, zero for MnN, FeN, CoN and NiN. Experimentally, FeN is reported to be antiferromagnetic (no moment given,[21] see also the section for $FeN_{0.91}$ later on), while CoN is reported to be paramagnetic (no moment given[20]). Recent Mössbauer measurements on $FeN_{0.91}$ in the

Table 2 Calculated data (spin-polarized) for ScN, TiN, VN, CrN, MnN, FeN, CoN and NiN

			Metal–nitrogen interactions			Metal–metal interactions		
Compound	Structure type	a/pm	Distance/ pm	$-$ICOHP/ eV atom^{-1}	$-$ICOHP/ eV bond^{-1}	Distance/ pm	$-$ICOHP/ eV atom^{-1}	$-$ICOHP/ eV bond^{-1}
ScN	$Fm\bar{3}m$	446	223	10.75	1.792	315	1.03	0.086
	$F\bar{4}3m$	482	209	8.21	2.052	341	0.06	0.005
TiN	$Fm\bar{3}m$	424	212	16.08	2.680	300	3.65	0.304
	$F\bar{4}3m$	456	197	10.98	2.745	322	0.40	0.033
VN	$Fm\bar{3}m$	410	205	19.21	3.202	290	4.32	0.360
	$F\bar{4}3m$	442	191	12.94	3.235	312	0.68	0.057
CrN	$Fm\bar{3}m$	402	201	19.96	3.327	284	3.36	0.280
	$F\bar{4}3m$	430	186	14.14	3.535	304	0.61	0.051
MnN	$Fm\bar{3}m$	396	198	20.79	3.465	280	3.09	0.257
	$F\bar{4}3m$	425	184	15.67	3.918	301	0.55	0.046
FeN	$Fm\bar{3}m$	395	198	20.98	3.497	279	2.55	0.213
	$F\bar{4}3m$	420	182	16.16	4.040	297	0.36	0.030
CoN	$Fm\bar{3}m$	394	197	19.93	3.322	279	1.86	0.155
	$F\bar{4}3m$	422	183	15.49	3.873	298	0.17	0.014
NiN	$Fm\bar{3}m$	398	199	16.00	2.667	281	1.32	0.110
	$F\bar{4}3m$	428	185	14.08	3.520	303	0.05	0.004

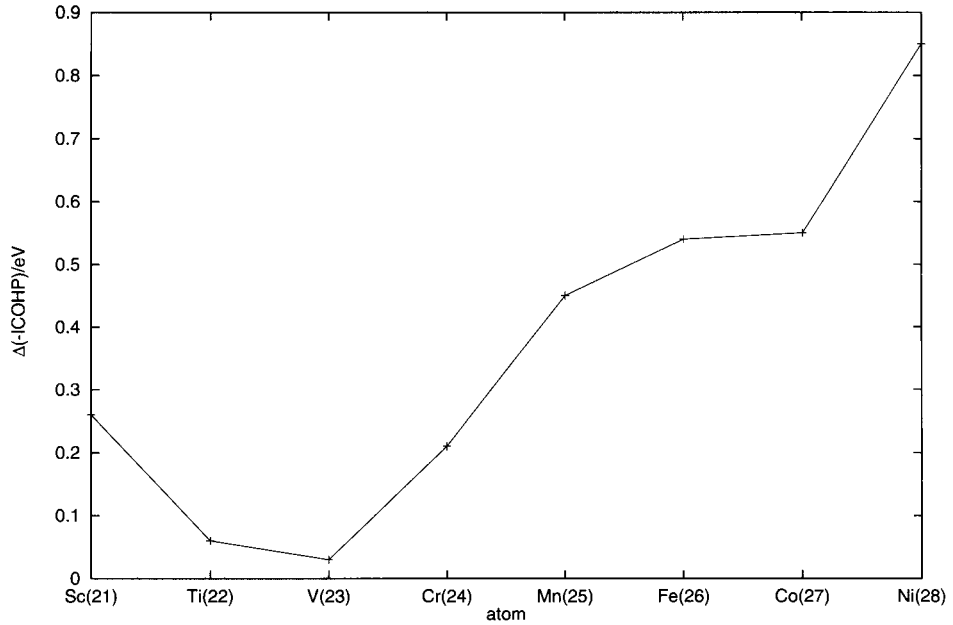

Fig. 3 The difference of the negative integrated COHP ($-$ICOHP) per metal–nitrogen bond between the zinc blende structure and the sodium chloride type against the atomic number; the positive numbers indicate by what amount a *single* bond is more stable in the zinc blende structure compared with the sodium chloride structure. See also Table 2.

zinc blende structure type by Nasu and Hinomura[25] nevertheless show that there are *no* magnetic hyperfine field splittings detectable at 10 K.

3.2 Iron nitrides

At least six different binary iron nitrides have been reported. We will start with the stoichiometric phases and move on to the non-stoichiometric ones.

3.2.1 ζ-Fe_2N. ζ-Fe_2N was synthesized by Rechenbach and Jacobs by flowing ammonia over iron powder.[26] The crystal structure of ζ-Fe_2N shows strong similarities to the anti-α-PbO_2 structure type. There is a distorted hcp arrangement of iron atoms, with the nitrogens occupying corner- and edge-sharing distorted octahedra (see Fig. 4) and with two iron–nitrogen bonds at 189 pm, another two at 196 pm, and finally two at 201 pm. There are also 12 iron–iron distances within the range 272–281 pm.

The DOS of ζ-Fe_2N, calculated using the experimental structure, is shown in Fig. 5. The large DOS at ε_F strongly suggests metallic character for this phase, in agreement with

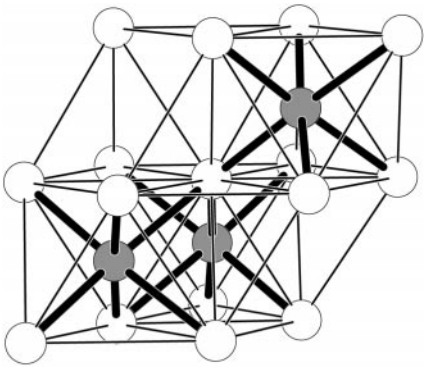

Fig. 4 Crystal structure of ζ-Fe_2N; shown is the anti-cuboctahedron of iron with three edge sharing nitrogen octahedra which form infinite one-dimensional chains.

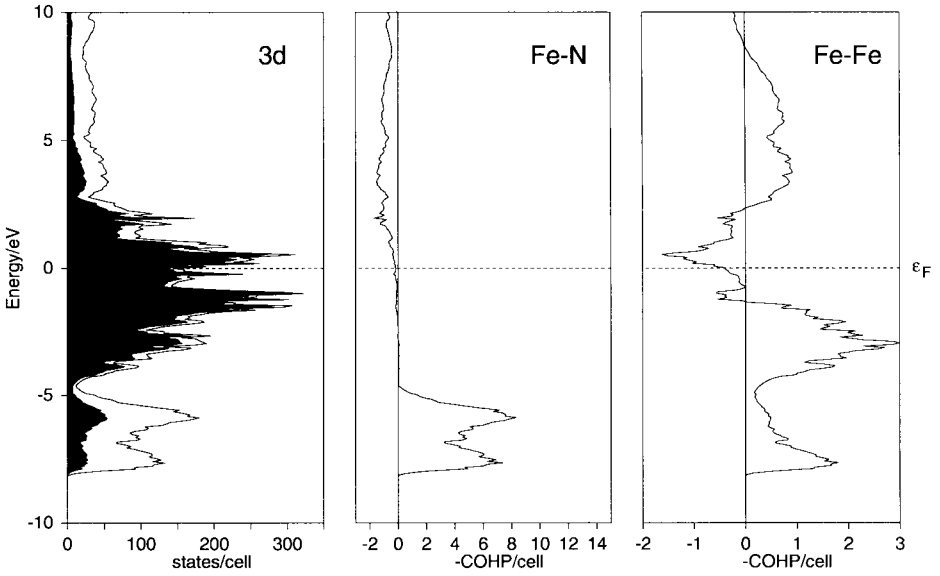

Fig. 5 Density-of-states (DOS) and local 3d projections (left), and the Crystal Orbital Hamilton Populations for the iron–nitrogen (middle) and iron–iron interactions (right) in ζ-Fe_2N.

the experimental result. The projection of the 3d states (black filling of the DOS curve) show that these orbitals dominate the states close to the Fermi level. The COHP analysis for the iron–nitrogen interactions (see also Fig. 5) shows strong Fe–N bonding between -8 and -5 eV and makes it clear that metal–nitrogen bonding is the driving force for forming the crystal, as expected. The presence of strong covalent bonding between the iron and nitrogen atoms explains the unusually small volume increments calculated for N^{3-} in these compounds.[27] The iron–iron bonding is also strong, with weaker antibonding interactions just below ε_F. The spin-polarized calculations give 1.5 unpaired electrons on the iron atom, fitting the experimentally observed paramagnetism.[28]

3.2.2 ε-Fe_3N. ε-Fe_3N was also synthesized by Jacobs *et al.* by nitridation of iron powder under flowing ammonia;[29] the crystal structure is hexagonal (Fig. 6). The iron atoms form a slightly distorted hcp packing, with the nitrogen atoms occupying only corner-sharing octahedra. The nitrogen atom is six-fold coordinated by iron atoms and the iron–nitrogen bond length is 193 pm. In addition, there are 12 close iron–iron distances which are 2×264 pm, 4×266 pm, 2×273 pm, and finally 4×274 pm.

The c/a ratio of the lattice constants was held constant during the optimization of the lattice parameters. We arrived at values of $a=446$ pm and $c=414.8$ pm. These are in satisfactory agreement with the experimental data (Table 3), with a difference of 5.1%. As for ζ-Fe_2N, the DOS of ε-Fe_3N in Fig. 7 shows metallic behavior, broad bands, and dominant iron 3d contributions at the Fermi level. Moreover, we also find strong iron–nitrogen and somewhat weaker iron–iron bonding (see COHP analysis in Fig. 7), with small iron–iron antibonding contributions at the Fermi level. This similarity, especially between the iron–iron COHPs of ζ-Fe_2N and ε-Fe_3N might have been expected from the analysis of structural relations between those two structures by Rechenbach and Jacobs.[26] The spin-polarized calculations give 1.6 unpaired electrons on the iron atom, which is in good agreement with the experimental result of 1.3–1.5 μ_B per iron atom.[30]

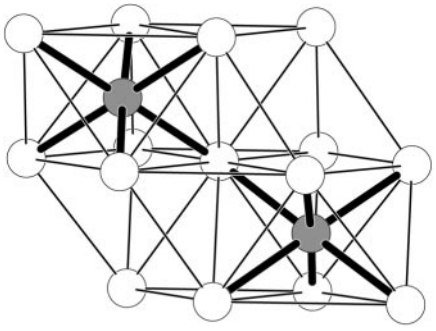

Fig. 6 Crystal structure of ε-Fe_3N; shown is the anti-cuboctahedron of iron with two corner sharing nitrogen octahedra.

3.2.3 γ′-Fe_4N. γ′-Fe_4N was synthesized by Jacobs *et al.* by reaction of iron powder with supercritical ammonia in high pressure autoclaves.[29] The crystal structure can be appropriately described by an antiperovskite structure incorporating two crystallographically different iron atoms (Fig. 8). Atom Fe(1) is linearly coordinated by two nitrogens with a bond distance of 190 pm while Fe(2) has 12 nearest Fe(1) neighbors at 268 pm. Nitrogen, on the other hand, is octahedrally coordinated by Fe(1) at 190 pm.

Theoretical optimization of the cubic lattice parameter gives $a=370$ pm, too short by only 2.4% when compared with the experimental value of 379 pm.

The DOS and the local 3d projections of Fe(1) and Fe(2) are given in Fig. 9. In agreement with experiment, the material is metallic, as found by Jacobs *et al.*[29] It is worthwhile mentioning the difference in electronic functionalities between Fe(1) and Fe(2), solely arising from the extreme difference in coordinations. While Fe(1) is responsible for the chemical bonding to nitrogen, thus showing strong dispersion in the DOS, Fe(2) experiences metallic twelve-fold coordination and moderate interactions with its Fe(1) neighbors, such that the Fe(2) dispersion is less than half of that of Fe(1).

Similar results can be deduced from the COHP curves shown in Fig. 10. The iron–nitrogen bonding originates almost exclusively from the Fe(1)–N interactions between -9 and -6 eV where Fe(2) does not mix in. On the energy scale, iron–iron bonding is nicely separated, at *ca.* -4 to -1 eV. Like in the other stable phases discussed previously, iron–iron antibonding effects are almost nonexistent below ε_F.

At first, the spin-polarized calculations within the local spin density approximation using 455 irreducible k points arrived at a total of 1.6 unpaired electrons. This average value is the approximate mean of the two individual spin occupations of 1.2 for Fe(1) (3×) and 3.0 for Fe(2) (1×). Surprisingly, this is below the experimental value of 2.21,[31] and even below

Table 3 Crystallographic and theoretical data for various binary iron nitrides

Compound	Space group	Wyckoff sites	Experimental				Theoretical		
			a/pm	b/pm	c/pm	μ_B	a/pm	c/pm	μ_B
FeN[21]	$F\bar{4}3m$	Fe: 4a N: 4c	430.7			AF[a] or 0	420		0
ζ-Fe_2N[26]	$Pbcn$	Fe: 8d (0.249, 0.128, 0.083) N: 4c ($y=0.364$)	443.73 (2)	554.13 (1)	484.29 (1)	para[b]	–		1.5
ε-Fe_3N[29]	$P6_322$	Fe: 6g ($x=0.3249$) N: 2c	469.19 (4)		436.70 (4)	1.3–1.5	446	414.8	1.6
γ'-Fe_4N[29]	$Pm\bar{3}m$	Fe(1): 3d Fe(2): 1b N: 1a	379.00 (6)			2.21	370		2.4
α''-$Fe_{16}N_2$[34]	$I4/mmm$	Fe(1): 4d Fe(2): 4e ($z=0.3125$) Fe(3): 8h ($x=0.25$) N: 1a	572.00		629.00	2.5 (3.5)	—		2.4
γ''-$FeN_{0.91}$[22]	$F\bar{4}3m$	Fe: 4a N: 4c	433			1.7 or 0	421		0
γ'''-$FeN_{0.5-0.7}$[22]	$Fm\bar{3}m$	Fe: 4a N: 4b	450			ferro[c]	386 378	($FeN_{0.75}$) ($FeN_{0.5}$)	1.52 1.62

[a]AF = antiferromagnetic. [b]para = Paramagnetic. [c]ferro = Ferromagnetic.

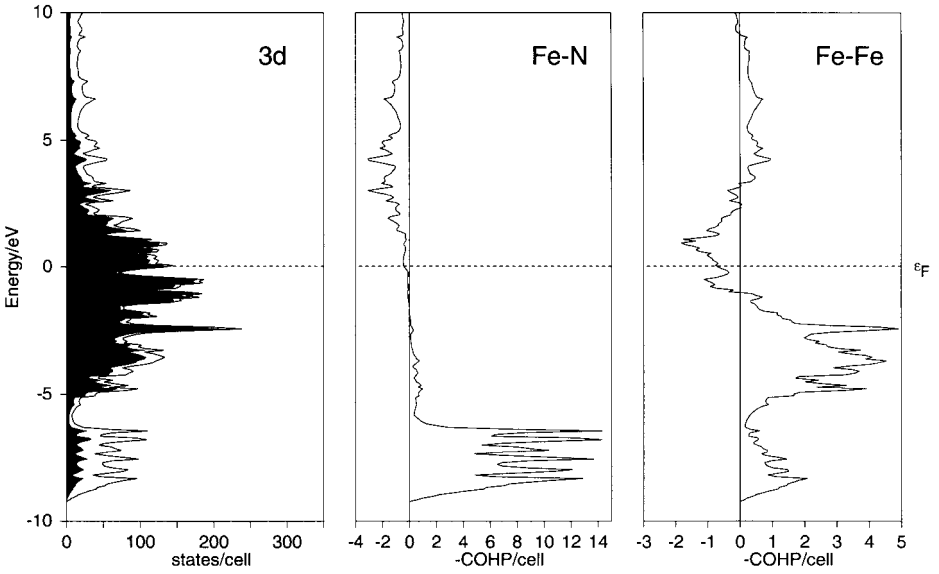

Fig. 7 Density-of-states (DOS) and local 3d projections (left), and the Crystal Orbital Hamilton Populations for the iron–nitrogen (middle) and iron–iron interactions (right) in ε-Fe_3N.

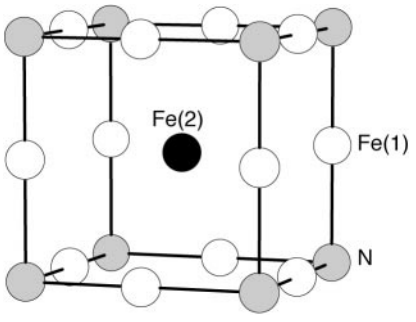

Fig. 8 Unit cell of γ'-Fe_4N.

similar calculations using the LMTO method, which also revealed values of 2.2.[32,33] We have repeated those calculations by Sakuma[33] and still arrived at values very close to our present results. Only when repeating the calculations with a much smaller number of k points were Sakuma's results reproduced. Then, however, the calculations are by no means converged, neither with respect to total energy nor magnetism.

Nevertheless, applying gradient corrections of the Perdew–Wang type and the full set of 455 irreducible k points

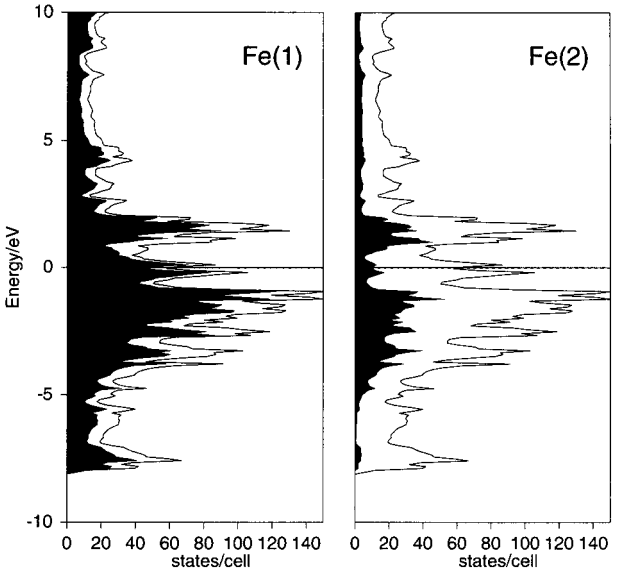

Fig. 9 Density-of-states (DOS) and local 3d projections of Fe(1) and Fe(2) for γ'-Fe_4N.

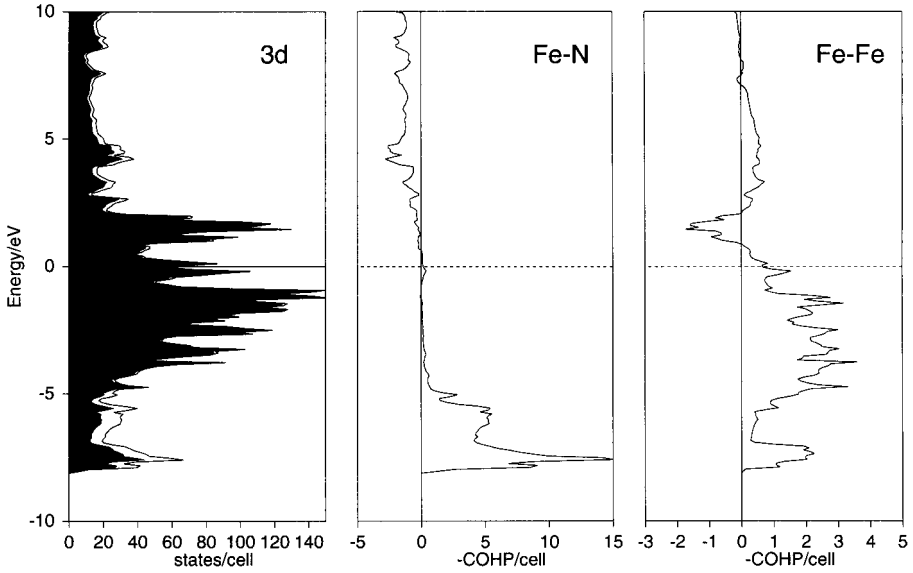

Fig. 10 Density-of-states (DOS) and local 3d projections (left), and the Crystal Orbital Hamilton Populations for the iron–nitrogen (middle) and iron–iron interactions (right) in γ'-Fe_4N.

finally leads to 2.2 unpaired electrons for Fe(1) and 3.1 for Fe(2). This gives an average of 2.4 unpaired electrons which is close to the experimental value. Note that Fig. 9 and 10 have been generated with the Perdew–Wang corrections.

3.2.4 α''-$Fe_{16}N_2$. The most iron-rich nitride phase discussed here, α''-$Fe_{16}N_2$, was first synthesized by Jack[34] by tempering N-martensite. Other possible methods have been reported.[35] A cubic structure was described by Jack as early as 1950.[36] The compound is currently of considerable interest since some have reported it to exhibit a very high magnetic moment (up to 3.2 μ_B), and a number of theoretical calculations have already been published.[37,38] All of them arrive at a magnetic moment of *ca.* 2.4 μ_B, which is in good agreement with most experimental results of 2.5 μ_B.[38]

The crystal structure of α''-$Fe_{16}N_2$ is shown in Fig. 11; in the very center there is an octahedrally coordinated nitrogen atom with two apical bonds of 195 pm [Fe(2)] and four equatorial bonds of 202 pm [Fe(3)]. Atom Fe(1) is coordinated only by iron [8×256 pm to Fe(3), 4×288 pm to Fe(2)]. Atom Fe(2) experiences four nearest Fe(3) atoms with an extraordinarily small distance of 235 pm, one Fe(2) atom at 239 pm, four next nearest Fe(3) atoms at 281 pm, and four Fe(1) at 288 pm. Finally, there is Fe(3) which has two nearest Fe(2) atoms at 235 pm distance, four Fe(1) atoms at 256 pm, again two Fe(2) atoms at 281 pm, and then four Fe(3) atoms at 286 pm.

Based upon the experimental structure, the DOS and the local 3d projections of Fe(1), Fe(2) and Fe(3) in α''-$Fe_{16}N_2$ are given in Fig. 12.

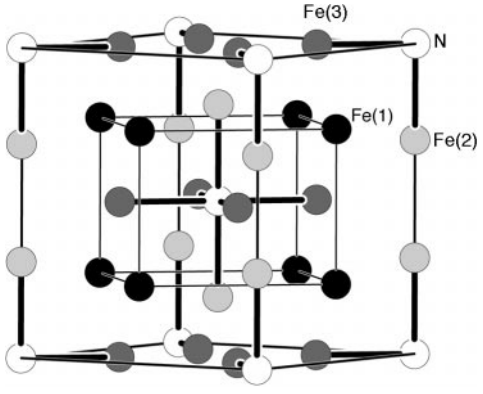

Fig. 11 Crystal structure of α''-$Fe_{16}N_2$.

The DOS, the iron–nitrogen and the iron–iron COHPs are shown in Fig. 13. In the iron–iron COHP the six iron–iron bonds of Fe(3) which are shorter than 260 pm dominate the curve around the Fermi level. The electronic difference between the three crystallographically different iron atoms is also reflected in their spin occupations. Atom Fe(1), which has no direct contact with any nitrogen atom, has 2.9 unpaired electrons, while Fe(2) and Fe(3) have 1.9 and 2.4, respectively, leading to a total number of 2.4 unpaired electrons. This finding for the Fe(1) atom is in accord with the result for the Fe(2) atom of γ'-Fe_4N which showed roughly the same number (3.0 or 3.1).

Another interesting observation comes from the COHP curves of α''-$Fe_{16}N_2$. While the overall iron–nitrogen bonding (Fig. 13) does not show any behavior that is different from the other binary iron nitrides, the iron–iron COHP is surprising. Here we do not find any antibonding iron–iron interactions up to the Fermi level. In fact, there are some *bonding* interactions above ε_F. Recall that even pure α-Fe has small iron–iron antibonding interactions below ε_F [Fig. 14 (left)]. An iron bcc lattice, which is modeled to match the subcell of the α''-$Fe_{16}N_2$ cell ($a = 286$ pm, $c = 314$ pm), already shows these novel bonding interactions above the Fermi niveau. In α''-$Fe_{16}N_2$, the iron–iron bonding is mainly due to the interaction of Fe(3) with its nearest Fe(1) (4×256 pm) and Fe(2) (2×235 pm) neighbors, while the second nearest neighbors with distances of > 280 pm do not lead to further bonding interactions. We conclude that the distortion of the iron bcc motif in α''-$Fe_{16}N_2$ leads to an upward shift of antibonding interactions above the Fermi level. In fact, the distortion is so large that potentially bonding interactions are lost, too. It may be worth reinvestigating the crystal structure of α''-$Fe_{16}N_2$.

3.2.5 γ''-$FeN_{0.91}$. Films of this non-stoichiometric binary phase have been synthesized by Takahashi *et al.* using the rf-sputtering technique.[22] According to their results, γ''-$FeN_{0.91}$ crystallizes in the zinc blende type with an experimental lattice constant of 433 pm. Our own theoretical optimization of the lattice parameter yields a value of 421 pm, too small by *ca.* 2.7%. This small underestimation of the lattice constant is typical for the local-density approximation. Moreover, we stress that our optimization is based on a stoichiometric 1 : 1 composition such that a comparison with the experimental

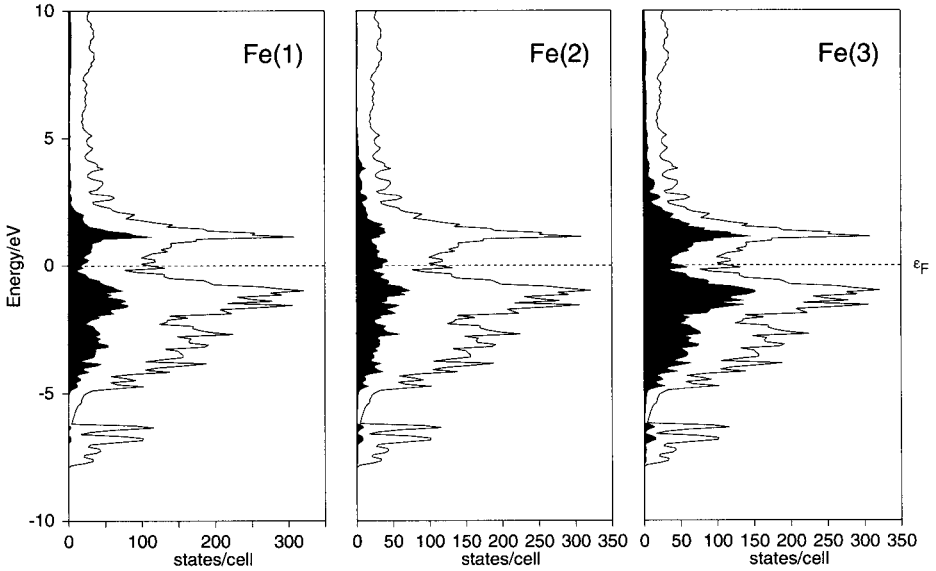

Fig. 12 Total DOS of α''-$Fe_{16}N_2$ with local projections for Fe(1), Fe(2) and Fe(3).

value of 430 pm (synthesis of the fully stoichiometric phase[21]) seems to be more appropriate; the error then is only *ca.* 2%.

The DOS of the stoichiometric phase has already been shown in Fig. 2, reflecting metallic character. This is in good agreement with the observations by Takahashi *et al.* We emphasize that the amount of antibonding iron–nitrogen interactions (four bonds of 182 pm) at the Fermi level is small while bonding interactions between the iron atoms (twelve distances of 297 pm) are insignificant (Fig. 2). Additional theoretical calculations performed in the spin-polarized mode revealed no tendency for unpairing of electrons whatsoever.

This finding is in conflict with the results found by Takahashi *et al.*[22] who detected a magnetic moment of *ca.* 1.7 μ_B. We believe that this discrepancy probably goes back to the slightly different stoichiometries (experimentally $FeN_{0.91}$ instead of theoretically FeN). It is also possible that additional γ'''-FeN_x impurity in that particular sample may have led to the non-zero magnetic moment. It is not easy to obtain pure γ''-$FeN_{0.91}$ free from a slight contaminant of the magnetic γ'''-$FeN_{0.5-0.7}$. The latter preparation requires substrate cooling to increase the yield of γ''-$FeN_{0.91}$.

3.2.6 γ'''-FeN_x ($x=0.5$–0.7). A film of this compound has also been made recently by Takahashi and coworkers using radiofrequency (rf)-sputtering.[22,39] Based on X-ray data measurements, the authors proposed that γ'''-$FeN_{0.5-0.7}$ adopts a NaCl type structure in which an fcc lattice of iron atoms also contains octahedrally coordinated nitrogen atoms, statistically distributed among the octahedral sites. As an alternative to this structure, the Mo_2N structure type where the nitrogen atoms occupy the octahedral positions in an ordered fashion was considered.

With respect to the iron/nitrogen atomic ratio, it is worthwhile mentioning that two of the stoichiometric iron nitride phases discussed above, ζ-Fe_2N and ε-Fe_3N, have similar Fe : N ratios.

3.2.7 Nitrogen contents in non-stoichiometric iron nitrides. Both structures suggested for γ'''-$FeN_{0.5-0.7}$ contain fcc arrangements of iron atoms. The stoichiometric phases ζ-Fe_2N and ε-Fe_3N not only have different iron arrangements (hcp), but also show distortions from ideal packing. In the following, we investigate the reasons if and why γ'''-$FeN_{0.5-0.7}$ may

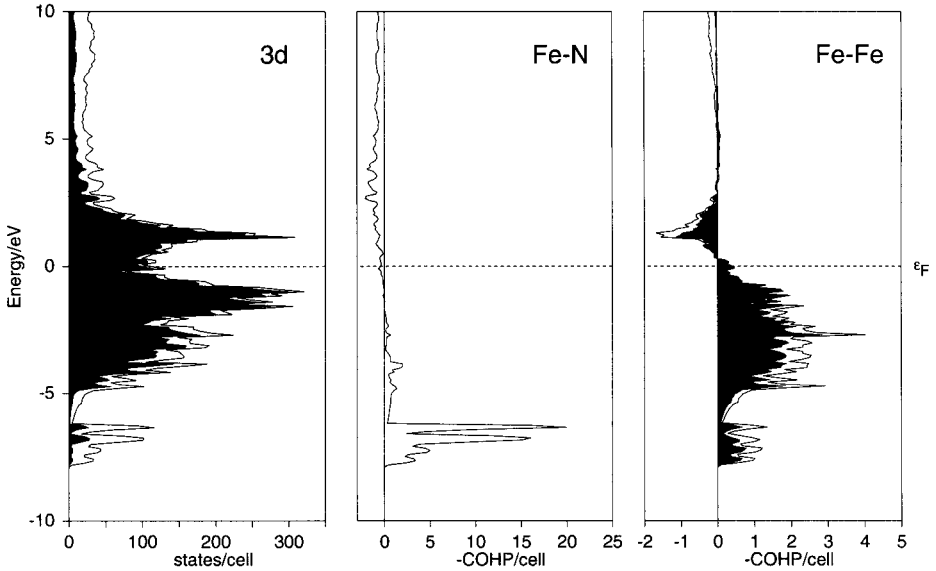

Fig. 13 Density-of-states (DOS) and local 3d projections (left), and the Crystal Orbital Hamilton Populations for the iron–nitrogen interactions (middle) and the iron–iron interactions (right) in α''-$Fe_{16}N_2$. The filled part in the iron–iron interactions are the six iron–iron bonds of Fe(3) shorter than 260 pm.

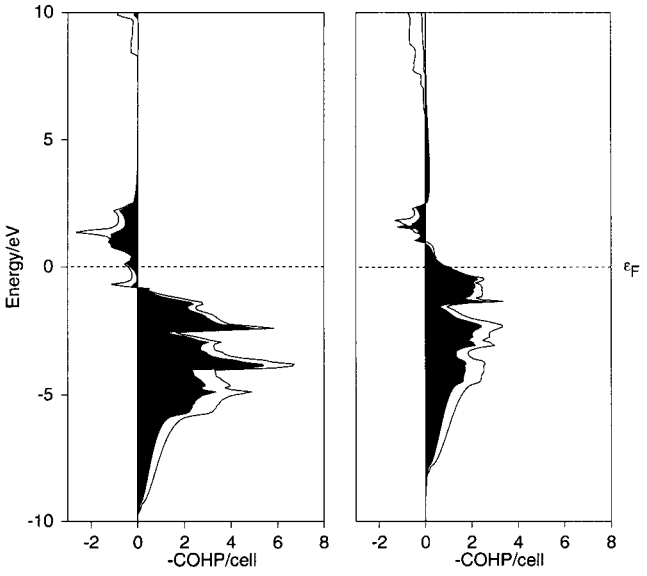

Fig. 14 Crystal Orbital Hamilton Populations for the eight nearest and six second nearest iron–iron interactions for α-Fe with an optimized lattice constant of 274 pm (left) and a bcc like iron lattice (right) that has been blown up and stretched in the z direction by 10% ($a=286$ pm, $c=314$ pm) to match a subcell found in α″-$Fe_{16}N_2$. The filled curves are the projections of the nearest eight neighbors, respectively.

crystallize with an fcc packing by means of several model calculations. To do so, we calculated a number of hypothetical iron nitrides with varying nitrogen contents, assuming a defect sodium chloride structure type throughout.

The electronic structure of FeN in the sodium chloride structure was discussed above. Nitrides $FeN_{0.75}$ (Fe_8N_6) and $FeN_{0.5}$ (Fe_8N_4) were studied in a structure where the unit cell of sodium chloride was doubled in z. In order to simulate the nitrogen defects, we used tetragonal space group symmetry, and the structure for Fe_8N_6 is shown in Fig. 15. During optimization of the lattice parameter, the c/a ratio was kept fixed at 2. No further spatial optimizations of the atomic positions were performed.

With decreasing nitrogen contents, the optimized lattice constants decrease monotonously. For FeN we found $a=395$ pm (see above), while $a=386$ pm is found for $FeN_{0.75}$, and $a=378$ pm for $FeN_{0.5}$. For γ′-Fe_4N ($\equiv FeN_{0.25}$) we found $a=370$ pm. The average number of unpaired electrons calculated for these structures are 1.27 for FeN, 1.52 for $FeN_{0.75}$, and 1.62 for $FeN_{0.5}$. Thus, we are confident to assign an average of *ca.* 1.5 unpaired electrons to the non-stoichiometric phase γ‴-$FeN_{0.5-0.7}$. This is consistent with the experiments of Heiman and Kazama who found Fe_xN_{1-x} ($0.40<x<0.75$) to be ferromagnetic.[40]

The DOS, iron–nitrogen, and iron–iron COHP curves are given in Fig. 1 for FeN (NaCl structure type), in Fig. 16 for Fe_8N_6 and in Fig. 17 for Fe_8N_4; as has been stated previously, the latter two calculations were based on an ordered defect NaCl structure type. The DOSs for the three different structures and stoichiometries show the expected behavior. For the lower nitrogen contents, the local environments of the iron atoms begin to differ, reflected by the broader DOS curves. All three hypothetical compounds clearly exhibit metallic character while the states near the Fermi level are, once again, iron-dominated.

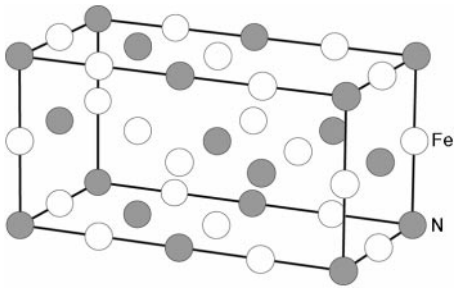

Fig. 15 Model structure of Fe_8N_6.

The COHPs for all three compounds exhibit significant Fe–N bonding interactions although they are somewhat smaller than for ε-Fe_3N and ζ-Fe_2N. The reductions can be traced back to some antibonding effects just below the Fermi level, only weakly seen for ζ-Fe_2N (see Fig. 5 for comparison). Thus, the distortions in the iron arrangements in ζ-Fe_2N have effectively reduced the antibonding effects. There is no distortion of the iron packing in ε-Fe_3N, and so one also can see the antibonding interactions just below the Fermi level (Fig. 7). Numerically, the negative integrated values of the Crystal Orbital Overlap Populations (−ICOHPs) up to the Fermi level are the following: for a single octahedron around nitrogen (six bonding interactions) we arrive at 31.7 eV for ε-Fe_3N, 21.2 eV for ζ-Fe_2N, 19.0 eV for Fe_8N_4 (undistorted Fe_2N), 23.4 eV for Fe_8N_6 (undistorted $Fe_{1.33}N$), 21.0 eV for FeN in the sodium chloride structure, and 16.2 eV for FeN in the zinc blende structure type.

The negative integrated values of the 12 nearest neighbor iron–iron COHPs are 12.6 eV for ε-Fe_3N, 7.6 eV for ζ-Fe_2N, 2.6 eV for Fe_8N_4 (undistorted Fe_2N model), 6.7 eV for Fe_8N_6 (undistorted $Fe_{1.33}N$ model), 2.6 and 0.36 eV for FeN in the sodium chloride and zinc blende structure type, respectively. ζ-Fe_2N is clearly preferred to Fe_8N_4; the iron–nitrogen and the iron–iron interactions are both stronger for the distorted iron lattice of ζ-Fe_2N. The value of the iron–nitrogen interaction in Fe_8N_6 is again stronger than for ζ-Fe_2N and Fe_8N_4, and the values decrease for FeN in sodium chloride structure type. The iron–iron interactions show a similar trend.

We now consider the experimental lattice parameter of γ‴-$FeN_{0.5-0.7}$ which was determined to lie at 450 pm. Recalling the theoretically optimized lattice parameters which were 395 pm for FeN, 386 pm for $FeN_{0.75}$ (Fe_8N_6 model) and 378 pm for $FeN_{0.5}$ (Fe_8N_4 model), all of them are far from the above experimental value. However, the theoretical lattice parameters relate very well with, for example, that of the even more nitrogen-deficient phase γ′-Fe_4N ($FeN_{0.25}$, see above) which is 379 pm. On the other hand, a lattice parameter of >400 pm is found for nitrogen-rich FeN in the zinc blende structure type only. Thus, we suggest that the lattice parameter of γ‴-$FeN_{0.5-0.7}$ needs to be redetermined. Taking in account that theoretically optimized lattice parameters are typically too short by 2–5%, a reasonable prediction for γ‴-$FeN_{0.5-0.7}$ would fall in the range 378–386 pm (plus 2–5%) *i.e. ca.* 389–398 pm, depending on the actual nitrogen content and assuming an ordered NaCl defect variant. These arguments neglect any thin film as well as substrate effects, the latter which may have forced γ‴-$FeN_{0.5-0.7}$ to adopt the sodium chloride type structure.

4 Conclusions

We have investigated all binary 1:1 first row transition metal nitrides by means of first principle band structure calculations. By successively filling up the bands with electrons, antibonding metal–metal interactions become more and more significant. Since these interactions are much weaker in the zinc blende structure type than in the sodium chloride structure type, the latter transition metal nitrides FeN and CoN crystallize in the zinc blende type. Based upon the bonding analysis, we predict that MnN should also appear in the zinc blende structure type. For NiN the analysis is more complicated although the many occupied antibonding levels make us doubt the stability of the binary 1:1 nickel nitride.

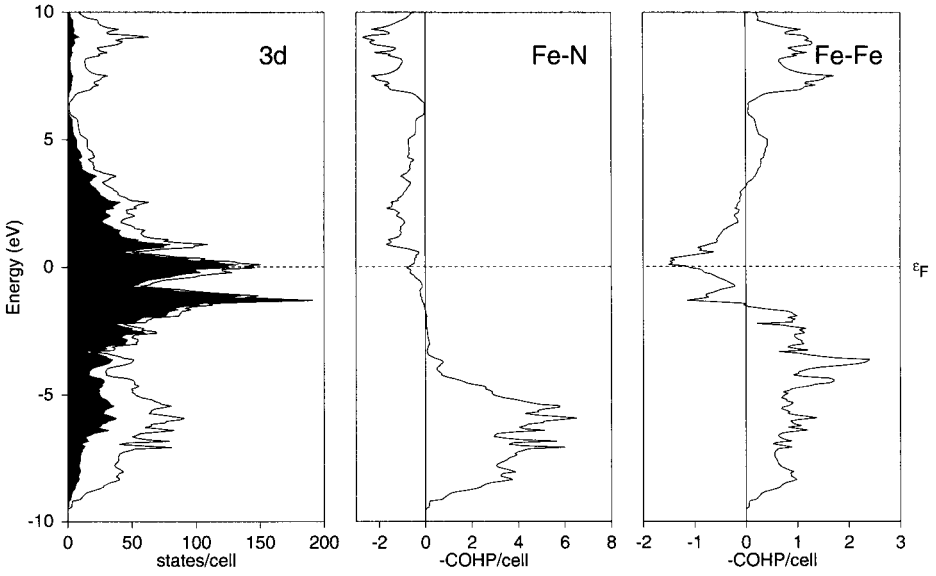

Fig. 16 Density-of-states (DOS) and local 3d projections (left), and the Crystal Orbital Hamilton Populations for the iron–nitrogen (middle) and iron–iron interactions (right) in hypothetical Fe_8N_6 (NaCl type structure).

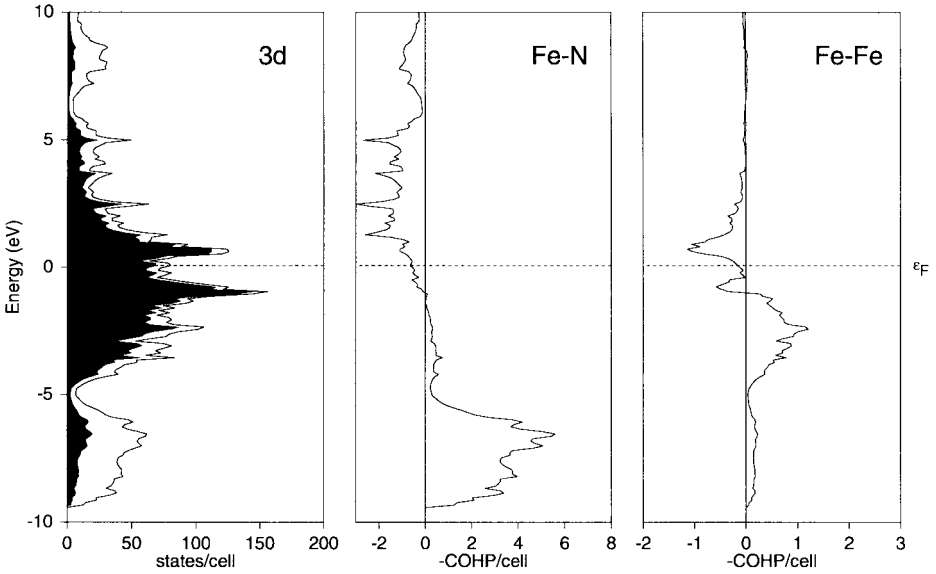

Fig. 17 Density-of-states (DOS) and local 3d projections (left), and the Crystal Orbital Hamilton Populations for the iron–nitrogen (middle) and iron–iron interactions (right) in hypothetical Fe_8N_4 (NaCl type structure).

For the case of the binary iron nitrides, we have been able to reproduce the measured ground state properties where experimentally available. COHP analysis reveals the importance of antibonding interactions for local structural distortions.

With respect to the nonstoichiometric phases, a number of model calculations lead to surprising results concerning structure and magnetism. The magnetic data of γ''-$FeN_{0.91}$ as well as the structural information of γ'''-$FeN_{0.5-0.7}$ possibly need to be reinvestigated.

Acknowledgement

The authors would like to gratefully acknowledge financial support from the New Energy and Industrial Technology Development Organization (NEDO, Japan) under Project Grant MB2: 'Advanced Nitrides: Novel Approaches, Electrical and Magnetic Properties, and Related Theoretical Calculations.'

References

1 K. Jack, *Proc. R. Soc. London, Ser. A*, 1948, **195**, 34.
2 O. K. Andersen, *Phys. Rev. B*, 1975, **12**, 3060.
3 H. Skriver, *The LMTO Method*, Springer-Verlag, Berlin, 1984.
4 O. K. Andersen, in *The Electronic Structure of Complex Systems*, ed. P. Phariseau and W. M. Temmerman, Plenum, New York, 1984.
5 J. Korringa, *Physica*, 1947, **13**, 392.
6 W. Kohn and N. Rostoker, *Phys. Rev.*, 1954, **94**, 1111.
7 P. Hohenberg and W. Kohn, *Phys. Rev. B*, 1964, **136**, 864.
8 W. Kohn and L. Sham, *Phys. Rev. A*, 1965, **140**, 1133.
9 U. von Barth and L. Hedin, *J. Phys. C*, 1972, **5**, 1629.
10 P. Blöchl, O. Jepsen and O. K. Andersen, *Phys. Rev. B*, 1994, **49**, 16223.
11 O. K. Andersen and O. Jepsen, *Phys. Rev. Lett.*, 1984, **53**, 2571.
12 G. Krier, O. Jepsen, A. Burkhardt and O. K. Andersen, The TB-LMTO-ASA program, version 4.7, Stuttgart.
13 R. Dronskowski and P. E. Blöchl, *J. Phys. Chem.*, 1993, **97**, 8617.
14 T. Hughbanks and R. Hoffmann, *J. Am. Chem. Soc.*, 1983, **105**, 3528.
15 R. Hoffmann, *Solids and Surfaces: A Chemist's View of Bonding in Extended Structures*, VCH, Weinheim, 1988.

16 K. Becker and F. Ebert, *Z. Phys.*, 1925, **31**, 268.
17 A. Christensen, *Acta Chem. Scand.*, *Ser. A*, 1978, **32**, 89.
18 J. Fitzmaurice, A. Hector and I. Parkin, *J. Chem. Soc.*, *Dalton Trans.*, 1993, 2435.
19 R. Blix, *Z. Phys. Chem. B*, 1929, **3**, 229.
20 K. Suzuki, T. Kaneko, H. Yoshida, H. Morita and H. Fujimori, *J. Alloys Compd.*, 1995, **224**, 232.
21 K. Suzuki, H. Morita, T. Kaneko, H. Yoshida and H. Fujimori, *J. Alloys Compd.*, 1993, **201**, 11.
22 M. Takahashi, H. Fujii, H. Nakagawa, S. Nasu and F. Kanamaru, in *Proceedings of The Sixth International Conference on Ferrites*, The Japan Society of Powder and Powder Metallurgy, Tokyo, Kyoto, 1992, p. 508.
23 J. Häglund, G. Grimvall, T. Jarlborg and A. Fernandez Guillermet, *Phys. Rev. B*, 1991, **43**, 14400.
24 A. Fernandez Guillermet and K. Frisk, *J. Alloys. Compd.*, 1994, **203**, 77.
25 S. Nasu and T. Hinomura, *Mater. Jpn.*, 1997, **36**, 35.
26 D. Rechenbach and H. Jacobs, *J. Alloys Compd.*, 1996, **235**, 15.
27 W. Biltz, *Raumchemie der festen Stoffe*, Leopold Voss, Leipzig, 1934.
28 J. Bainbridge, D. Channing, W. Whitlow and R. Pendlebury, *J. Phys. Chem. Solids*, 1973, **34**, 1579.
29 H. Jacobs, D. Rechenbach and U. Zachwieja, *J. Alloys Compd.*, 1995, **227**, 10.
30 M. Robbins and J. White, *J. Phys. Chem. Solids*, 1964, **25**, 717.
31 C. Guillaud and H. Crevaux, *C.R. Acad. Sci.*, 1946, **222**, 1170.
32 S. Ishida and K. Kitawatase, *J. Magn. Magn. Mater.*, 1992, **104–107**, 1933.
33 A. Sakuma, *J. Magn. Magn. Mater.*, 1991, **102**, 127.
34 K. Jack, *Proc. R. Soc. London, Ser. A*, 1951, **208**, 216.
35 K. Jack, *J. Alloys Compd.*, 1995, **222**, 160.
36 K. Jack, *Acta Crystallogr.*, 1950, **3**, 392.
37 R. Coehoorn, G. Daalderop and H. Jansen, *Phys. Rev. B*, 1993, **48**, 3830.
38 H. Sawada, A. Nogami, T. Matsumiya and T. Oguchi, *Phys. Rev. B*, 1994, **50**, 10004.
39 S. Kikkawa, M. Fujiki, M. Takahashi, F. Kamamaru, H. Yoshioka, T. Hinomura, S. Nasu and I. Watanabe, *Appl. Phys. Lett.*, 1996, **68**, 2756.
40 N. Heiman and N. Kazama, *J. Appl. Phys.*, 1981, **52**, 3562.

Paper 8/09935I